The Voronoi Polyhedra as Tools for Structure Determination in Simple Disordered Systems

J. C. Gil Montoro* and J. L. F. Abascal

Departamento de Química Física, Facultad de Ciencias Químicas, Universidad Complutense de Madrid, E-28040, Spain

Received: September 15, 1992

The structure of some simple fluids is analyzed through the Voronoi tessellation of the configurations generated by computer simulation. Special emphasis is put on the investigation of disordering, i.e., the deviation from solid-state properties. The models studied include a simple Lennard–Jones (LJ) liquid, two quenched states obtained from the liquid, and a system made of noninteracting particles (the ideal gas), while a state point corresponding to the LJ solid phase is used as reference. To perform the Voronoi construction, an algorithm specially suited for disordered systems is presented. The arrangement of particles has been studied through the geometrical features of their Voronoi polyhedra (VP). It is shown that two parameters can give a description of the VP in such a way that the disordering of the system is clearly manifested. One is the volume distribution coefficient of skewness, and the other is the shape of the VP as described by the convex bodies nonsphericity factor. In particular, the clusters present in a rapidly quenched liquid are easily revealed in this way.

1. Introduction

The characterization of the spatial structure of a system is a challenging matter far from being solved. The usual description through the radial distribution function $g(r)$ is not enough because the one-dimensional nature of $g(r)$ implies that 3D correlations have been averaged out. Some aspects of the global structure may be depicted by obtaining the power expansion in spherical harmonics of the neighborhood of a particle[1] or inspecting the relative intensity of the components of the structure factor,[2] but those approaches are rather indirect and thus are difficult to interpret. A more straightforward insight can be achieved by focusing our attention in the Voronoi polyhedra (VP)[3] associated with each atom. The VP, defined as the convex region of space closer to its central atom than to any other, are a generalized version of the Wigner–Seitz cells in crystallography (see, for example, ref 4). As the structure of liquids and amorphous solids is primarily determined by repulsive forces[5] and these are produced by nearest neighbors, it follows that the description of the shape and size of the VP may be used to characterize that structure.

Such an analysis was first employed by Bernal[6] to the case of a random packing system. After that it has been applied in the framework of structural determination in a wide variety of physicochemical problems such crystallization,[7-11] glass formation,[12,13] solvation structure,[14] defects in melting transition,[15] solvolytic reactions,[16] molecular volumes of proteins,[17,18] studies on neighboring identities,[19] interfacial area between substrate and enzyne,[20] and determination of clefts in receptor structures.[21,22]

For the description of the VP both shape and size of the individual polyhedra should be given. The volume distribution has been widely used as a measure of size but there is no general agreement about how to describe the shape: "signature" of the polyhedra[7] (enumeration of the number of faces with three, four, and so on vertices), number of faces distribution,[9,11] portion of odd-edged faces,[10] dimensionless parameter constructed with surface and area,[10,23] and even "tetrahedricity" and "octahedricity" of the related Delaunay tetrahedra.[24] But the scaled particle theory (SPT)[25] demonstrated some time ago that a suitable parameter to define the shape of a convex body is the so-called nonsphericity, also referred to as anisotropic factor, α which is

given by

$$\alpha = \frac{RS}{3V} \tag{1}$$

V, S, and R being the volume, surface, and average curvature radius of the convex body, respectively. This parameter is the unity for a sphere and greater for any other convex body.

In this work we show how the combined analysis of volume and nonsphericity of the VP is a powerful tool to study the structure of disordered fluids. We apply this technique to the Lennard–Jones fluid at two thermodynamic points corresponding to solid and liquid phases, two differently quenched supercooled states obtained from the liquid, and the ideal gas (i.e., a noninteracting system obtained by randomly placing particles into a box). The structural features of each system are clearly disclosed by the volume and nonsphericity distributions as shown below.

In section 2 we describe the algorithm we have developed to obtain the Voronoi construction. Section 3 addresses the simulations and quenching procedures, while the results and discussion are presented in section 4. Some concluding remarks will be given at the end of the paper.
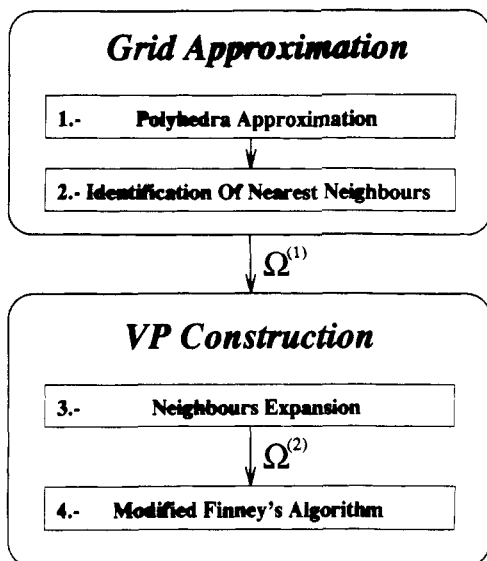
2. The Voronoi Tessellation Algorithm

The 3D Voronoi construction is a nontrivial problem for which a few algorithms have been proposed.[26-29] In all cases, for a given atom i, one needs to select a set Ω of N_Ω neighboring atoms. For this set to be valid it must include all of the so-called *nearest* neighbors, $\dot{\Omega}$, formed by the $N_{\dot{\Omega}}$ particles strictly needed to define the faces of the VP

$$\dot{\Omega} \subset \Omega \tag{2}$$

The efficiency of the different algorithms is given in terms of N_Ω. Therefore, the key is to select the set Ω as small as possible; ideally, N_Ω should be equal to $N_{\dot{\Omega}}$ so that Ω only contains the nearest neighbors. Traditionally, Ω has been built as a list of *closest* neighbors (using a cutoff radius) which is a good approach (in the absence of other information) for any system with a quite *isotropic* neighborhood (say, a solid or even a liquid) but which turns out to be a poor approximation to $\dot{\Omega}$ for more disordered systems (such as glassy states or electrolyte solutions): to include the $N_{\dot{\Omega}}$ nearest neighbors, a rather large cutoff distance must be chosen and consequently the number of atoms in Ω increases. In fact, we decided to face the problem in a completely new way when we noticed that for some ill-behaved systems (the nonin-

---

* Author to whom correspondence should be addressed.

Grid Approximation

1.- **Polyhedra Approximation**

2.- **Identification Of Nearest Neighbours**

$\Omega^{(1)}$

VP Construction

3.- **Neighbours Expansion**

$\Omega^{(2)}$

4.- **Modified Finney's Algorithm**

Figure 1. Flow chart of the proposed algorithm for the Voronoi polyhedra construction.

Figure 2. Location of neighbors through the grid and overlapping polygons as a consequence of a missing edge (see the text).

teracting and even more the quenched states) sometimes a nearest neighbor was so far away that we were forced to increase the cutoff up to almost half the simulation box length. The construction of a "direct" polyhedron[26] (built using only some of the closest atoms which suffice to close it) gives for each particle an upper limit for the cutoff radius which includes all its nearest neighbors, but the situation is not better because for those systems the radii are very large. Besides, the direct polyhedron is also quite difficult to obtain.

Our algorithm is designed to avoid the inherent problems associated with the use of a cutoff distance. Instead, we explore the space surrounding each particle in such a way that the local *anisotropy* is directly incorporated into the algorithm. Figure 1 is a flow chart of the algorithm. It is made up of two main blocks, namely the grid approximation and the VP's construction, which in turn are subdivided in two steps.

The Grid Approximation. The system is divided in boxes with the use of a grid. Each box delimited by the grid is assigned to its closest particle so that the set of boxes ascribed to one particle approximates its VP. (A 2D example is given in Figure 2. There, a small region of a system is depicted. The edges of the Voronoi polygons are drawn as solid lines and the approximation obtained through the grid as dotted lines. The grid itself is not plotted for the shake of clarity). The most obvious—and inefficient—way of performing the assignation of boxes is computing the distances from each box to every particle. Instead, in our procedure, each particle "conquers" the boxes around its previously occupied boxes beginning with that in which the particle is located. Only when a box is disputed between two particles do we need to evaluate the distances and assign the box to the closest one. When there are no free boxes, the polyhedra approximation phase (step 1 of Figure 1) finishes. Notice that certain properties of the VP can be directly estimated from these approximated VP, as is the case of the volume. Only if one is interested in, say, the VP surface or its number of faces is it necessary to go further and obtain the true VP.

In stage 2 the algorithm identifies the nearest neighbors of each particle. By definition, two particles are nearest neighbors if their VP's are adjacent. Thus, the approximated VP trivially provide the nearest neighbors of each particle: two particles are nearest neighbors if at least two boxes, one of each, are adjacent. This is the main advantage of our method as opposed to the use of a cutoff-based list which furnishes the closest (not necessarily nearest) neighbors. It is worth noting that the grid approximation can be very efficiently handled as only integer arithmetic is
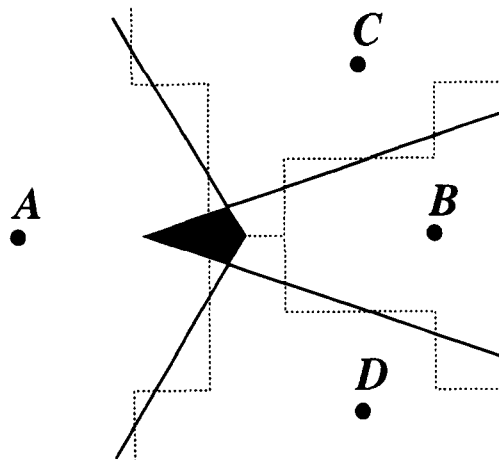
required (all the distances involved in stage 1 are computed in terms of "boxes").

Since we have the nearest neighbor sets for *all* the particles in the system, Ω_i, it follows that by simple inspection of the neighborhood lists we can extract the common neighbors' tetrads, i.e., the subsets of four atoms so that each one is a neighbor of the others. These tetrads are nothing but the vertices of the so-called Delaunay tetrahedra, and the VP are easily obtained since its vertices are just the circumcenters of the Delaunay tetrahedra.

Rigorously, as described, the algorithm only works in the limit of zero thickness grid; a finite thickness grid may result in missing in Ω some far nearest neighbors (which define small area VP faces, as that between particles A and B in Figure 2) or even in including non-nearest neighbors (as is the case of particles C and D in the same figure). The implications and solution for this failure are given in the next subsection.

The VP Construction. In this block we describe how to obtain the VP from an *approximate* set of nearest neighbors $\Omega_i^{(1)}$. Firstly, we should be able to include the missing nearest neighbors. We will refer to this step as *neighbor expansion* (step 3 in Figure 1). It is only intended to improve the efficiency of the whole algorithm since a high-resolution grid (which would detect all the nearest neighbors) would be too expensive in terms of computer time. Secondly, a procedure to remove the spurious neighbors introduced by previous stages is required. For this purpose we use a modification of Finney's algorithm[27] (step 4).

In the neighbor expansion phase, the atoms with a certain number N_{cn} of common neighbors with atom i are added to $\Omega_i^{(1)}$ giving an improved set $\Omega_i^{(2)}$. For example, in Figure 2, the grid approximation fails to locate B as neighbor of A, as said above. However, if we expand the A neighbors with $N_{cn} = 2$ (the most likely choice for a two-dimensional system) B will be included in $\Omega_A^{(2)}$ because both C and D belong to both $\Omega_A^{(1)}$ and $\Omega_B^{(1)}$; i.e., we can build two bridges between A and B through common neighbors. The price one has to pay for adding most of the nonpreviously detected neighbors is the possibility of inclusion of fake ones, which must be eliminated later.

Now, one could take for each particle the current neighbors set $\Omega_i^{(2)}$ as the list of candidates Ω_i and proceed with any standard algorithm such as the one by Tanemura et al.[28] or Medvedev.[24] We chose to modify Finney's algorithm[27] in order to improve its efficiency. In Finney's procedure the circumcenters of the tetrahedra built connecting all the possible combinations of four atoms (the central one and three other among the Ω members) are computed; the VP vertices are those circumcenters closer to the central atom than to any other in Ω. Finney's method is not specially suitable unless the number of particles N_Ω in the approximate set is close to $N_{\hat\Omega}$. But we can cross the neighborhood
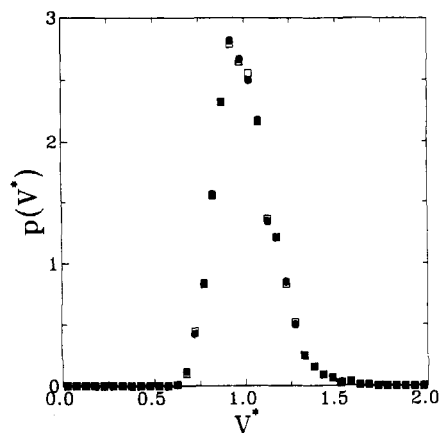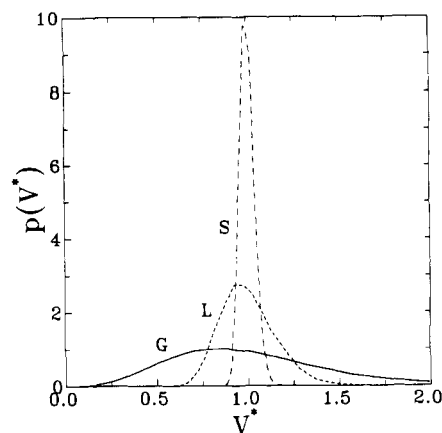
Figure 3. Voronoi polyhedra volumes distribution for the Lennard–Jones liquid with two different sampling grids: □, 20 × 20 × 20; ●, 80 × 80 × 80.

Figure 4. Voronoi polyhedra volume distribution functions about the mean for the solid (S), liquid (L), and gas (G) systems.

information between particles to eliminate most of the tetrads not leading to a real VP vertex. All the atoms defining a Delaunay tetrahedra are nearest neighbors of each other. Thus, to build the VP of particle i we do not need to try all the three-atom combinations among its nearest neighbors list, but only those being nearest neighbors among them. But as our $\Omega_i^{(2)}$ does not exactly fit the Delaunay network, we need to relax this condition somewhat. Thus, we do not input to Finney's algorithm all the combinations of three atoms from $\Omega_i^{(2)}$ but only those with a given number of "neighborhood links", say 1 or 2, among them. In this way, the N_Ω^3 dependence of Finney's algorithm is greatly improved.

The main advantage of the algorithm is its robustness. Provided a reasonable grid is to be used, the initial set $\Omega^{(1)}$ furnished by the grid ensures that a (closed) polyhedron can be obtained irrespective of the disordering degree of the system. Nevertheless, it is possible that two nearest neighbors were not identified either by the grid approximation or by neighbor expansion. In that case, the resulting VP is missing a face. The two polyhedra which should share that face are bigger than the correct ones because a small region of space is assigned to both. In our example of Figure 2 the shaded area would be the surface ascribed to both the A and B polygons if these two atoms were not considered neighbors, i.e., with no neighbor expansion. These approximate VP's are very close to the true ones with most of the geometrical quantities (volume, surface, total edge length, and average curvature radius) being almost the same, except of course the number of faces. Figure 3 compares the polyhedra volume distribution for several configurations of the 108-particle Lennard–Jones liquid described in the next section using two sampling grids (20 and 80 boxes per dimension, respectively) with no neighbor expansion ($N_{cn} = 0$). The departures are acceptable even for such rough grid. Besides, even if our algorithm may generate slightly overlapping polyhedra this can be easily checked. As the total sum of the VP volumes for any configuration should match the simulation cell volume and overlapping polyhedra always have volumes bigger than the true VP volume, the difference between the total VP and cell volumes is therefore a measure of the correctness of the tessellation. Our experience is that an error of 0.1% in the total volume for our 108-particle systems gives completely satisfactory results for all the properties of the polyhedra studied in this paper.

3. The System and Its Simulation

Microcanonical molecular dynamics (MD) simulations were performed with a sample of 108 particles in standard periodic boundary conditions using a fifth-order predictor–corrector algorithm and the Lennard–Jones 12-6 potential shifted at 2.5σ. We chose the thermodynamic states $T = 2.74\epsilon/k_B$, $\rho = 0.65/\sigma^3$

(L, liquid far from the triple point) and $T = 0.68\epsilon/k_B$, $\rho = 1.0/\sigma^3$ (S, solid). The equations of motion were integrated with a time-step of $0.001 \ (m\sigma^2/\epsilon)^{1/2}$. 6500 configurations were generated after equilibration, among which 500 were saved for later analysis.

Two quenched states were generated through a standard Monte Carlo (MC) procedure with $T = 0$ applied to every saved liquid configuration which ensures a descent of each particle to a local energy minimum. 100 attempted moves per particle with a constant displacement of 0.7σ—resulting in a global acceptance rate of 6%—were employed to originate the first quenched (Q_1) state, which corresponds to a moderate distortion of the liquid. State Q_2 was obtained by attempting to move each particle 500 times. Beginning with $\Delta r = 0.7\sigma$, the displacement was continuously reduced to keep the acceptance rate about 40%, so that at the end the moves are vanishingly small. The so-obtained state Q_2 corresponds to the *proper structure* of the liquid as termed by Naberukhin et al.[30]

The last studied system is a completely noninteracting fluid, the ideal gas, in which the particles are randomly distributed (G system). 1500 configurations were used in this case.

4. Results and Discussion

For all the systems the Voronoi construction using the algorithm described in section 2 has been built, the properties of the individual VP have been computed, and its distributions have been accumulated and averaged along the 500 (1500 for system G) configurations. In all cases, the maximum error accepted in the total volume due to possible overlapping VP produced by the algorithm was kept under 0.1% using a 40 × 40 × 40 grid for the S system, 50 × 50 × 50 for the L system, and 80 × 80 × 80 for the Q_1, Q_2, and G systems.

Figure 4 displays the normalized VP volume distribution functions $p(V^*)$ for the S, L, and G systems. We chose to deal with V^*, the VP volume reduced with that of the perfect solid at the same density as a reference, so that different systems could be compared. The distribution would be a δ function for a perfect simple solid (the only VP present would be just the Wigner–Seitz cell). For our realistic solid model there is a very sharp peak centered just below $V^* = 1$. As previously reported,[9,11] most of the particles have little distorted VP's due to thermal vibrations about their equilibrium positions. The distribution is almost symmetric; only small fluctuations around the perfect solid VP occur. The L system shows a much more spread distribution though the maximum is not shifted substantially from that of the solid. The curve is slightly asymmetric, with detected VP volumes ranging from 0.55 to 1.85. The liquid particles are able to diffuse to some extent producing local areas of high/low density which correspond to small/big VP volumes. Of course, the enlargement of a polyhedra implies diminution of others but the
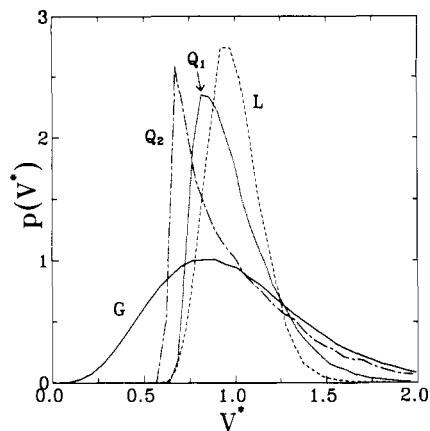
Figure 5. Voronoi polyhedra volume distribution functions about the mean for the quenched (Q_1 and Q_2), liquid (L), and gas (G) systems.

TABLE I: Volume Distribution Coefficients of Skewness for the Systems Considered

system	$m_{3/2}$	system	$m_{3/2}$
solid	0.242	quenched (1)	1.180
liquid	0.589	quenched (2)	1.345
gas	0.727		

total volume and the mean remain unchanged.

$$\int_0^\infty p(V^*)dV^* = \int_0^\infty V^* p(V^*)dV^* = 1 \qquad (3)$$

The VP volume distribution must be asymmetric as a consequence of the fact that there is no upper limit for the maximum volume of a VP may exhibit (except the obvious boundary given by the periodic conditions). Conversely, there is a lower limit because the steep repulsive forces bring out a nonpenetrable core with a volume roughly given by $\pi\sigma^3/6$. This also explains why the most probable volume has a value lower than unity. The G system shows a flat distribution because very small and big VP are possible as the particles are completely independent and the distribution entropy increases when the values spread over a wide range.

The quenched states volume distributions are plotted in Figure 5 which also displays the L and G curves for comparison. When the liquid is quenched the particles tend to aggregate and the number of small volume VP increases. As commented above, this implies that other VP must have larger volumes and the distribution becomes clearly asymmetric. The Q_1 curve shows the earlier stage of the quenching process. Compared with that of the liquid, the maximum shifts toward lower volumes while at the bigger volumes it becomes more flat but the peak value does not change significantly. In the final stage of quenching—the Q_2 state—all of the innermost particles of the dense clusters have approximately the same volume which is denoted by the sheer slope of the curve below the maximum. The outermost particles can have more or less neighbors so the slope of the VP distribution curve is progressively decreasing. In fact, the final part of the distribution is essentially coincident with that of the G system denoting the existence of low-density areas with almost isolated particles among the clusters.

The volume distribution coefficients of skewness given by

$$m_{3/2} = M_3/M_2^{3/2} \qquad (4)$$

where M_n is the nth moment about the mean, are summarized in Table I. Notice how the low-intensity quenched state Q_1 has twice the skewness of its originating liquid while the ideal gas takes up the central place. Therefore, this is a simple parameter which properly reflects the anisotropy of the neighborhood of the particles and clearly discriminates between systems.

For the evaluation of the nonsphericity parameter, α, the mean curvature radius, R, of the corresponding convex body must be
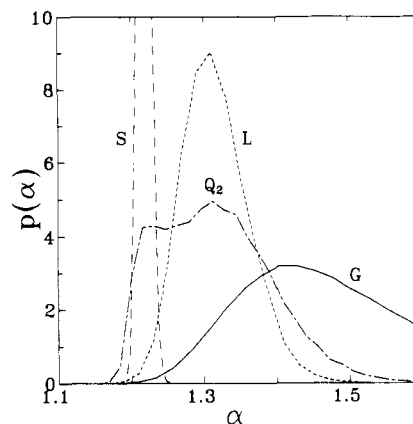
Figure 6. Voronoi polyhedra nonsphericity distribution for the systems studied. Curve labels as for previous figures.

known. For a polyhedron, R is given by[31]

$$R = \frac{1}{8\pi}\sum l_i\phi_i \qquad (5)$$

The sum extends over polyhedron edges of length l_i, and ϕ_i is the angle between the normal vetors to the intersecting faces. The nonsphericity distribution for all the systems studied is shown in Figure 6 (to avoid confusion only the quenched Q_2 state is drawn). The curve corresponding to the solid is extremely narrow, with a maximum at $\alpha = 1.223$. The probability of finding polyhedra with an anisotropic factor lower than that of the face-centered Wigner–Seitz cell ($\alpha_{fcc} = 1.117$) is negligible. We saw that the thermal motion of the particles in the solid system only slightly distorts the perfect lattice VP volumes. This distortion is clearly manifested in the displacement of the nonsphericity distribution which nevertheless remains very sharp. The L system $p(\alpha)$ is much more wide, and the value at the maximum is about six times lower than that of the solid (the heights peak ratio was only about 3.5 for the volumes distribution). Besides, the most probable anisotropic factor is located noticeably shifted from that of the S system, at about 1.31. In this sense, the α distribution distinguishes the fluid from the solid better than the volume distribution does. The VP for the G system have large nonsphericities, and the maximum of the curve is located at $\alpha = 1.42$. Ninety-two percent of the polyhedra have α greater than 1.31. The most illuminating curve is that corresponding to the Q_2 system. The distribution rapidly grows up and seems to reach a wide plateau for nonsphericites ranging from 1.20 to 1.37. At the top of the plateau a maximum identically aligned with that of the liquid one is distinguishable. The maximum for the solid system is also coincident with a small secondary maximum at the beginning of the Q_2 plateau. The quenched-state nonsphericity distribution can be explained in terms of a combination of "solid" and "liquid" polyhedra. This is clear if one realizes that the Q_2 curve can be accurately described by the sum of two asymmetric distributions—x^2 distributions with six (or more) degrees of freedom in particular—one centered at the position of the maximum of the S curve with height 4.2 and width at half height about 0.05 and the other centered along the liquid curve with height 5.0 and width 0.14.

Figure 7 portrays the face distribution results. These were obtained with suitable algorithm parameters in order to keep the error in volume well below 0.01%. The solid distribution agrees with published data for other states of the LJ solid.[9,11] In particular, the most probable polyhedron is that having 14 faces, two more than the face-centered Wigner–Seitz cell due to thermal motion. In our liquid there are nearly the same number of polyhedra having 15 and 14 faces, which is consistent with Hsu et al.,[11] who found more 14-face polyhedra in their LJ liquids not far from the fluid and solid coexistence region. The Q_1 system is midway from the liquid and the completely quenched Q_2 state
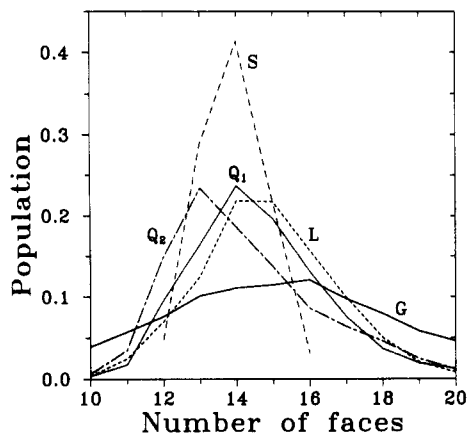
Figure 7. Voronoi polyhedra faces distribution for the systems studied. Curve labels as for previous figures.

for which 13- and 14-face polyhedra have almost the same probability denoting that the quenching procedure decreases the number of nearest-neighbors. It is clear that the face analysis hides most of the structural features of the systems. This is mainly due to the discreteness of the distribution but also to the fact that the same weight is given to a big face—shared between two very close neighbors—and to a small cut in a vertex produced by a particle which is much farther away. In this sense, the analysis using the signature of the polyhedra—which has been of great help in the investigation of crystal nucleation[8,9,13]—should surely be of little interest for describing the structure of more disordered systems. As shown in this work, the alternative may be the use of the nonsphericity parameter.

5. Concluding Remarks

We have developed and tested a new algorithm to perform the Voronoi construction of an arbitrary set of particles which is specially well suited for disordered systems. The algorithm has robustness as its main advantage. Provided a reasonable grid is used, a (closed) polyhedron is obtained irrespective of the disordering degree of the system. The improvements needed to obtain more refined results are also given and can be applied within the desired compromise between efficiency and accuracy. In fact, the results obtained for the number of faces distribution—the property less accurately computed with our algorithm—closely matches previously reported data.

We have shown that the use of the nonsphericity factor α describes the shape of the Voronoi polyhedra (VP) in such a way that the structure of the system is clearly revealed. For ordered systems such as solids and liquids we have found it superior to the traditionally used face-related quantities. But this is especially true as far as aggregation processes are involved so it can help in our understanding of disordered structures as quenched[32] or glassy states. Our current work on the structure of ions in electrolyte solutions[33] confirms this assert.

References and Notes

(1) Steinhardt, P. J.; Nelson, D. R.; Ronchetti, M. *Phys. Rev. B* **1983**, *28*, 784.

(2) Mandell, M. J.; McTague, J. P.; Rahman, A. *J. Chem. Phys.* **1976**, *64*, 3699.

(3) Voronoi, G. *Z. Reine Angew. Math.* **1908**, *134*, 199.

(4) O'Keefe, M. *Acta Crystallogr.* **1979**, *A35*, 772.

(5) Hansen, J. P.; McDonald, I. R. *Theory of Simple Liquids*; Academic Press: New York, 1986.

(6) Bernal, J. D. *Proc. R. Soc. London, A* **1964**, *280*, 299.

(7) Tanemura, M.; Hiwarati, Y.; Matsuda, H.; Ogawa, T.; Ogita, N.; Ueda, A. *Prog. Theor. Phys.* **1977**, *58*, 1079.

(8) Hsu, C. S.; Rahman, A. *J. Chem. Phys.* **1979**, *70*, 5234. Hsu, C. S.; Rahman, A. *J. Chem. Phys.* **1980**, *71*, 4974.

(9) Cape, J. N.; Finney, J. L.; Woodcock, L. V. *J. Chem. Phys.* **1981**, *75*, 2366.

(10) Nose, S.; Yonezawa, F. *J. Chem. Phys.* **1986**, *84*, 1803.

(11) Hsu, T.; Mou, C. *Mol. Phys.* **1992**, *75*, 1329.

(12) Tanaka, M. *J. Phys. Soc. Jpn.* **1986**, *55*, 3108.

(13) Watanabe, M. S.; Tsumuraya, K. *J. Chem. Phys.* **1987**, *87*, 4891.

(14) David, E. E.; David, C. W. *J. Chem. Phys.* **1982**, *76*, 4611. David, E. E.; David, C. W. *J. Chem. Phys.* **1982**, *77*, 3288. David, E. E.; David, C. W. *J. Chem. Phys.* **1982**, *77*, 6251. David, E. E.; David, C. W. *J. Chem. Phys.* **1983**, *78*, 1459.

(15) Allen, M. P.; Frenkel, D.; Gignac, W.; McTague, J. P. *J. Chem. Phys.* **1983**, *78*, 4206.

(16) Bellagamba, V.; Ercoli, R.; Gamba, A.; Simonetta, M. *J. Mol. Struct. THEOCHEM* **1985**, *123*, 383. Bellagamba, V.; Ercoli, R.; Gamba, A.; Simonetta, M. *J. Chem. Soc., Perkin Trans. 2* **1986**, 1127.

(17) Richards, F. M. *J. Mol. Biol.* **1974**, *82*, 1.

(18) Gellatly, B. J.; Finney, J. L. *J. Mol. Biol.* **1982**, *161*, 305.

(19) Baranyai, A.; Ruff, I. *J. Chem. Phys.* **1986**, *85*, 365.

(20) David, C. W. *Biopolymers* **1988**, *27*, 339.

(21) David, C. W. *Comput. Chem.* **1988**, *12*, 207.

(22) Lewis, R. A. *J. Comput. Aided Mol. Design* **1989**, *3*, 133.

(23) Ruocco, G.; Sampoli, M.; Vallauri, R. *J. Mol. Struct.* **1991**, *250*, 259.

(24) Medvedev, N. N.; Naberukhin, Y. I. *J. Non-Cryst. Solids* **1987**, *94*, 402.

(25) Gibbons, R. M. *Mol. Phys.* **1969**, *17*, 81.

(26) Brostow, W.; Dussault, J. P.; Box, B. L. *J. Comput. Phys.* **1978**, *29*, 81.

(27) Finney, J. L. *J. Comput. Phys.* **1979**, *32*, 137.

(28) Tanemura, M.; Ogawa, T.; Ogita, N. *J. Comput. Phys.* **1983**, *51*, 191.

(29) Medvedev, N. N. *J. Comput. Phys.* **1986**, *67*, 223.

(30) Naberukhin, Yu. I.; Voloshin, V. P.; Medvedev, N. N. *Mol. Phys.* **1991**, *73*, 917.

(31) Hadwiger, H. *Altes und Neues über konvexe Körper*; Birkhäuser Verlag: Basel, 1955.

(32) Habasaki, H.; Okada, I.; Hiwatari, Y. *Molec. Sim.* **1992**, *9*, 49.

(33) Gil Montoro, J. C.; Bresme, F.; Abascal, J. L. F. To be published.